International Journal of Medical, Medicine and Health Sciences
ISSN: 2517-9969
Vol:8, No:6, 2014

Preparation and Characterization of Newly Developed Trabecular Structures in Titanium Alloy to Optimize Osteointegration

M. Regis, E. Marin, S. Fusi, M. Pressacco, L. Fedrizzi

Abstract**—**Electron Beam Melting (EBM) process was used to prepare porous scaffolds with controlled porosity to ensure optimal levels of osteointegration for different trabeculae sizes. Morphological characterization by means of SEM analyses was carried out to assess pore dimensions; tensile, compression and adhesion tests have been carried out to determine the mechanical behavior. The results indicate that EBM process allows the creation of regular and repeatable porous scaffolds. Mechanical properties greatly depend on pore dimension and on bulk-pore ratio. Adhesion resistance meets the normative requirements, and the overall performance of the produced structures is compatible with potential orthopaedic applications.

Keywords**—**Additive manufacturing, orthopaedic implants, osteointegration, trabecular structures.

I. Introduction

THE success of bone response in prosthetic implant osteointegration processes largely depends on the surface properties of the applied material [1]. In this field, a large research work has been carried out to improve biological response of the human body to biomaterials, mainly related to enhance adhesion of bone osteoblast on the implant surface [1]-[5].

Particularly, the development of highly porous surfaces and scaffolds is of great interest, and its successful application is demonstrated by clinical evidences [6], [7]. There is a lot of interest in studying the ability of the natural bone to re-grow in narrow porosities cellular solids and metal foams [2], [6], [7].

According to what reported in the literature, pore size and porosity play a critical role in the formation of new bone tissue. In fact, it seems that a minimum pore size of 300µm has to be reached in order to improve osteointegration. Further, it has been found that the growth of osteoblast is quicker in 600µm holes than in other diameters, ranging from 300, 400, 500 to 1000µm [6].

In addition, bone response can be enhanced also by surface roughness. It has been demonstrated that micro-texturing enhances the osteointegration properties of the scaffold, at the point that comparable levels of bone ingrowth can be obtained even with different pore diameters and porosity [8], [9].

It has to be considered however that porosity and roughness affect the mechanical properties of the realized structures, and have to be appropriately designed for the mechanical safety of the overall prosthesis.

Moreover, the manufacturing techniques used to produce scaffolds and structures are often complex and not scalable at an industrial level.

According to the findings reported in literature, the desired maximization of bone ingrowth can be efficiently obtained by realizing porous components with Electron Beam Melting (EBM) technology [2], [8].

The EBM additive manufacturing technique has been extensively studied and applied in the prototyping of a wide range of industrial applications [10]-[13]. EBM process conditions allow realizing high melting point alloys components. The advantages of additive manufacturing in the production of porous scaffolds are related to high volume production capacity and process control, as well as to the possibility to easily modify the geometry of the produced structures, which is based on 3D CAD models [14].

One of the major examples in the production of highly porous orthopaedic components is Trabecular Titanium™ (TT). The EBM process creates single part components, in which TT is applied to the outer surfaces of acetabular cups to maximize bone response. TT is a porous structure with two mesh sizes, 640 and 1200 µm, both based on multi-planar hexagonal cells, and its morphology and properties have been designed for imitating the natural trabecular bone [15].

The titanium powder beads melted to realize the desired cellular solids naturally create roughness at a micro scale on the melted arms, and with a 640 or 1200µm open porosity both structures ensure high levels of osteointegration [8], [16]-[18]. TT is produced either in Ti6Al4V or in Ti cp Gr2, and is currently applied to acetabular components.

However, in different anatomical sites, trabecular dimensions may vary significantly, demanding a tailored porosity for an optimal bone ingrowth [19], [20].

The aim of this study is therefore to prepare Ti6Al4V Trabecular Titanium™ scaffolds with different pore dimensions, and test their morphological and mechanical properties, in order to provide new solutions designed for an optimal osteointegration of implants for every specific anatomic bone tissue and evaluating the possibility of their application in prosthetic components.

M. Regis is with Limacorporate S.p.A, Villanova di San Daniele, UD 33038 Italy (phone: +39 0432 945511; fax: +39 0423 945512; e-mail: marco.regis@limacorporate.com).

E. Marin is with the University of Udine, Udine, UD 33100 Italy (e-mail: elia.marin@uniud.it).

II. Materials and methods

A. Scaffold Design and Preparation

A CAD 3D modeler software was used to create three different structures on the basis of the same multi-planar hexagon of the TT cellular structures, applying a scale factor of 0.5, 0.75, or 1.25 on the original 640 µm TT base cell (Fig. 1). The cells were replicated in order to obtain a 3D matrix for each structure. Meshes were then cut with Boolean operators on planes and volumes to obtain the desired scaffold shapes.

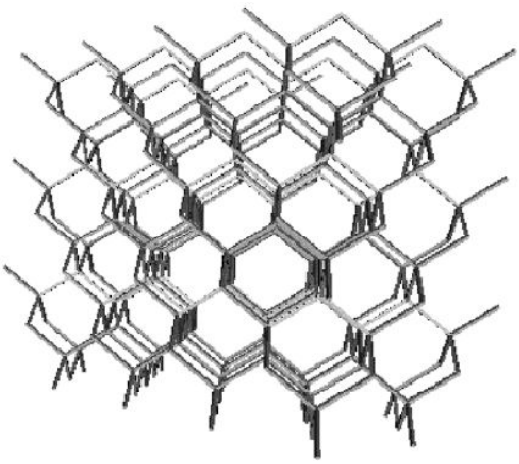

Fig. 1 Trabecular Titanium™ structure 3D model

For the characterization tests, cylinders of 10.5mm diameter and 11.2mm height have been used in compression tests and morphology evaluation, while dog-bone shaped specimens (13x6.7mm, 195mm length) have been realized for tensile test and 22.5x22.5mm square shaped sandwich structures were prepared for the adhesion test, in which a porous layer was inserted between two layers of bulk material (Fig. 2). Table I summarizes all the prepared specimens for the scaffolds characterization.

TABLE I
Prepared Specimens

Scaffold	Scale factor	Test	Dimensions
A	0.5	Compression / morphology	Ø10. 5 mm; h11.2 mm
		Tensile	13x6.7 mm; h 195 mm dog-bone shape
		Adhesion	22.5x22.5 mm
B	0.75	Compression / morphology	Ø10.5 mm; h11.2 mm
		Tensile	13x6.7 mm; h 195 mm dog-bone shape
		Adhesion	22.5x22.5 mm
C	1.25	Compression / morphology	Ø10.5 mm; h11.2 mm
		Tensile	13x6.7 mm; h 195 mm dog-bone shape
		Adhesion	22.5x22.5 mm;

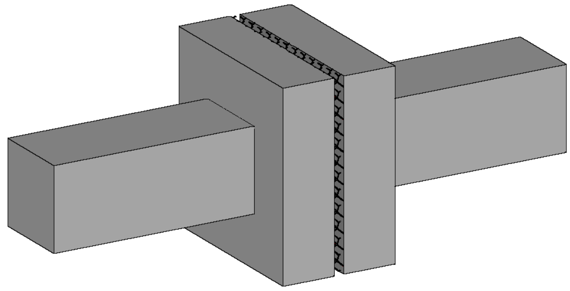

Fig. 2 Specimen for the adhesion test. A bulk-porous layer-bulk sandwich specimen was prepared, in order to evaluate the tear resistance of the scaffolds against a bulk substrate

B. Testing

Compression, tensile and adhesion tests were carried out using an MTS Landmark 370 uniaxial tensile testing machine, servo-hydraulically assisted, equipped with a 100 KN class 0.5-certified load cell. Tests were performed at a constant strain speed until failure or breakage of the specimens. Strength was calculated by dividing the applied load with the cross section of the tested specimens. Adhesion test was carried out according to what reported in the ASTM standard for coatings, for comparison purposes with previous studies [16], [21], even if, in this case, the manufacturing technique of the specimens does not produce coated structures but continuous monolithic components. Test is considered successful if fracture occurs within the porous layer of the sandwich structure and not at the interface between bulk and porous layer.

Morphology evaluation was performed using image post processor software for microscopes and Scanning Electron Microscopy (SEM) technique for image acquisition. The main issue of the pore dimension evaluation was related to the orientation angle of the measure. Since spatial position of the scaffold and its cutting plane determine the observed pore dimension, because the orientation of the structure affects the projection of the 3D porosity into the observation plane, samples were all evaluated by rotating the sample by fixed angles in order to expose the hexagonal plane passing through the two opposite vertices and the centre of gravity of the cellular element. SEM images were then taken and evaluated by the measurement software.

III. Results and discussion

Fig. 3 shows the SEM images of the evaluated porous structures. Scaffolds appear as high open porosity foams, with irregular shape of the melted material but with a great repeatability in terms of geometry and pore dimension, as observed elsewhere for the TT starting structure [16], [17]. Pore dimension measurements were reliable for all samples, showing a narrow data dispersion from the average value. This indicates a great regularity and repeatability of the EBM production process. The applied scaling factors result in the variation of the pore diameter and percentage difference from the average, but not in the thickness of the mesh arms. From

Table II, it can be seen that pore diameter is 143, 350 and 802µm for A, B and C structures, respectively, and that arm thickness remains almost unchanged.

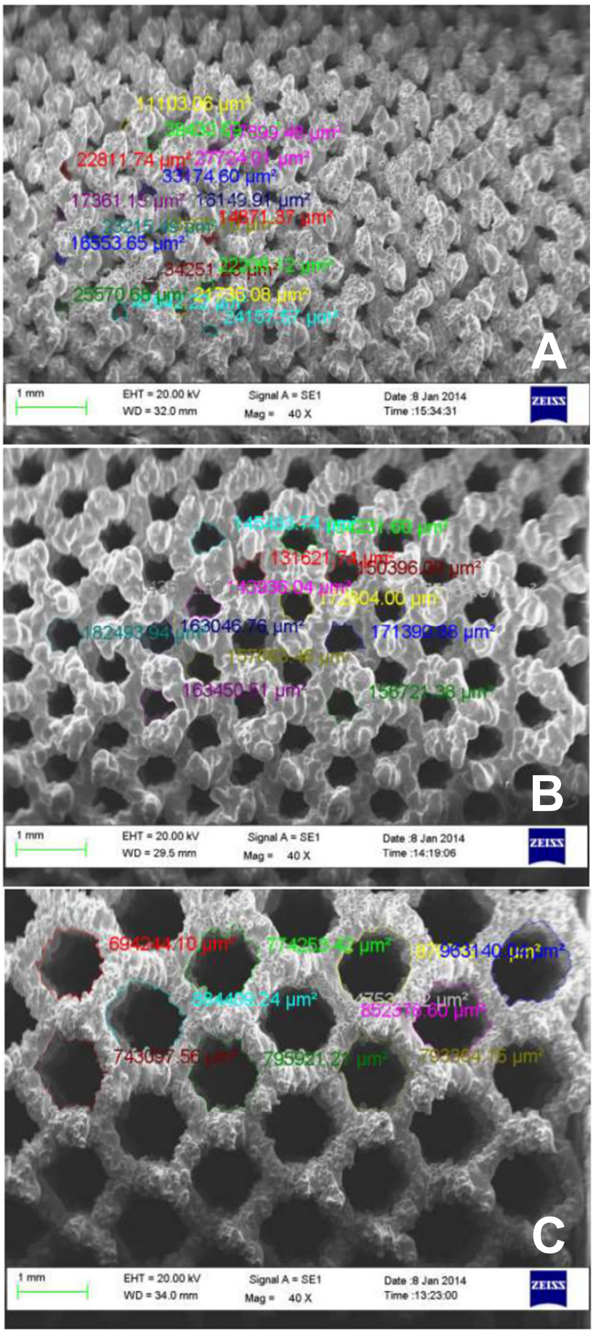

Fig. 3 From top to bottom, SEM images of A, B, and C scaffolds used to assess pore dimensions and arm thicknesses

TABLE II
PORE DIMENSION AND ARM THICKNESS

Scaffold	Pore dimension [µm]	Arm thickness [µm]
A	143 ± 30	348 ± 39
B	350 ± 16	366 ± 47
C	802 ± 38	350 ± 36

Arm thickness can be tuned by changing machine process parameters, to enhance or reduce the beam spot dimension and power. This will result in an enlarged or restricted melt pool area, modifying arm thickness and, consequently, porosity of the realized scaffold.

In order to increase pore dimension for structure A, a different set of process parameters was used for the sample production. The resulting sample (A*) pore dimension after the tuning was 230±29µm, indicating that even with an reduced melt pool area the machine precision cannot be less than ±250µm. (Fig. 4).

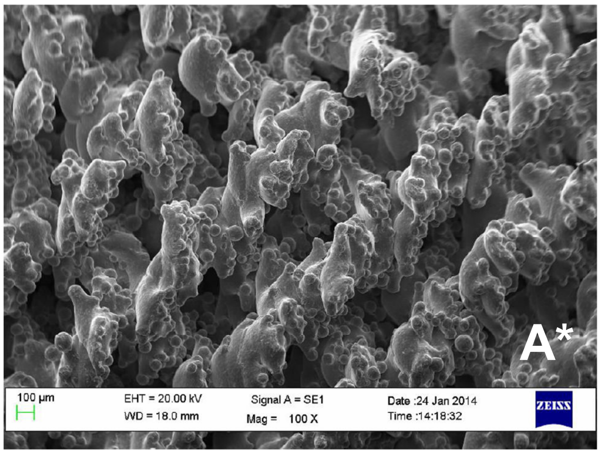

Fig. 4 Modified A scaffold with different EBM process parameters (A*)

From what emerges from the SEM images, it seems that forcing the machine process to reduce beam spot size will result in a partial fusion of powder beads, which remain present and distinguishable at the arm surface. Further work has to be carried out in order to properly optimize beam parameters in order to realize smaller structures. For this reason, only A, B and C structures were characterized with mechanical tests.

Mechanical characterization results are summarized in Table III. As predictable, the mechanical properties of the realized structures were different, since pore dimension and overall bulk-pore ratio varied among the scaffolds.

TABLE III
MECHANICAL PROPERTIES

Scaffold	Compressive peak stress [MPa]	Tensile peak stress [MPa]	Adhesion peak stress [MPa]
A	185.1 ± 5.8	124.7 ± 3	93.0 ± 2.2
B	73.2 ± 0.3	55.9 ± 2.4	76.6 ± 3.3
C	12.1 ± 0.2	7.5 ± 2.3	24.6 ± 2.0

The tensile, adhesion and compressive strength of the scaffolds was higher for smaller porosity dimensions, as predictable. Peak stresses differed greatly among the structures. Fig. 5 illustrates the mechanical behavior of the realized structures to tensile, compressive and adhesion loads. In the tensile test graph, stress-strain curves were nearly linear, indicating an elastic behavior for all specimens. Regarding the plastic deformation at ultimate loads, A structure showed a low ductility immediately before fracture, while for B and C specimens the plastic behavior was progressively more pronounced.

This is presumably due to the lower stiffness of the higher pore sized structures. In general, the limited plasticity of the porous structures is caused by the presence of a relatively small amount of arms in the resistant sections.

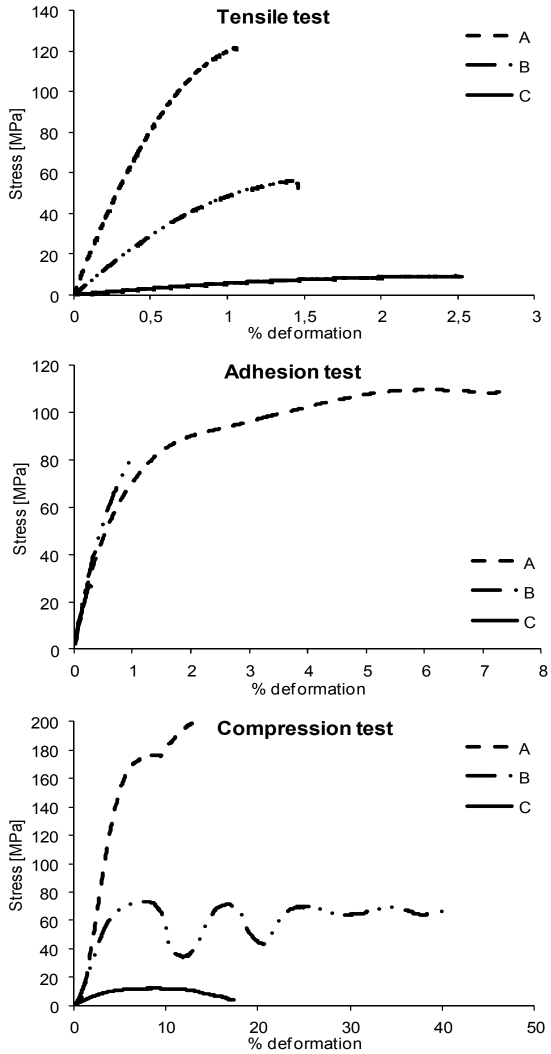

Fig. 5 From top to bottom, mechanical behavior in tensile, adhesion and compression tests for A, B and C scaffolds

At the beginning of the test, breakage of the first arms does not result in the failure of the whole structure, which occurs when a certain amount of arms along the weakest plane of the structure (with a 45° inclination) does break. When this condition is reached, the whole structure collapses instantaneously [22]. Deformation at break was 1.1, 1.5, and 2.5% for A, B and C structures, respectively.

Adhesion test gave similar indications, despite for A structure, which showed a long and well defined plateau stress. This can be attributed to the yielding in bending of the cell edges, which is usually observed in open cell foam structures [23]. Deformation at break was thus 8.5, 1.0, and 0.3% for A, B and C scaffold, respectively. For every specimen, fracture occurred within the net structure.

Differently from previous tests, the mechanical behavior observed under compression varied according to pore size of the tested structures. In fact, for smaller pore size, after the arms failure in the 45° weaker plane, indicated by the inflection point in the graph, the structure compacted and, acting as a bulk material, showed a further increase in the specimen resistance. This situation was not replicated for the bigger pore size scaffolds, which collapsed immediately after the failure at 45°, since the overall limited number of resistant arms and the modified loading conditions caused by the deformation of the metallic arms under loading (sample C).

For B structure, instead, after the failure of the 45° plane, cells showed a somewhat more complicated behavior which caused the stress to rise and fall steeply with increasing strain [23]. This is caused by the structure compaction, which occurs after the slipping of the resistant plane, resulting in the creation of additional resistant planes. This leads to the compressed structure resistance enhancement, and to the possibility for the scaffold to resist at larger strains.

The observed behavior was repeatable for all the tested samples. Data dispersion was limited as for full density materials, and peak stresses ranged from 12.1 MPa for C scaffold to 182.1 MPa for A scaffold.

The elastic, compressive and adhesion modulus were calculated for each tested scaffold. Values are reported in Table IV. In accordance to what observed for mechanical strength, Young's and compression moduli were higher for smaller structures. This will have an impact on the in vivo behavior of the scaffolds, since it is known that bone response is related also to stress shielding effects [24]. Adhesion modulus was almost constant among A, B and C scaffolds, indicating a great influence of the bulk structure in the elastic response of the specimens.

TABLE IV
ELASTIC MODULI

Scaffold	Compressive modulus [MPa]	Young's modulus [MPa]	Adhesion modulus [MPa]
A	45.5 ± 2.3	177.4 ± 2.7	109.8 ± 9.7
B	19.3 ± 0.3	59.3 ± 2.2	130.2 ± 2.1
C	2.4 ± 0.4	6.3 ± 0.4	112.8 ± 2.2

IV. CONCLUSION

The experimental results reported in this study indicate that the EBM process ensures the realization of highly accurate porous scaffolds, with narrow variations of pore dimension and geometry. The powder melting process results in a natural irregularity of the realized trabeculae, modifying the original CAD geometry towards a micro-textured arm appearance. The prepared structures have shown to be sensitive to scaling factors applied to the 3D model in terms of pore dimensions, while it was observed that arm thickness strongly depends on the process parameters set up rather than to the original geometry.

By modifying the EBM process parameters however, the melted structures can be prone to fusion defects which can cause a premature failure of the scaffolds. As a consequence, mechanical properties can be varied safely by tuning pore dimensions, limiting the arm thickness modification only to a certain extent. The EBM process accuracy is therefore assessed at ±250μm.

Mechanical properties depend on pore dimensions, both in terms of peak stresses and deformation at break. Larger pore diameter results in lower strength and higher ductility of the structure. In each of the tested structures, mechanical resistance to adhesion has shown to meet the minimum requirements for a potential use in prostheses [21].

Compression behavior is greatly changing according to material density. Progressive enhancement of compressive resistance is ensured if a proper bulk-pore ratio is reached. Lower bulk-pore ratios will result in weaker structures, while higher bulk-pore ratios will make the scaffold act as a bulky material, enhancing significantly not only its resistance but also its elastic modulus. This can play a role in the choice of the newly developed net structure to be used in orthopaedic implants.

Although osteointegrative potential and biological fixation of the realized structures has to be assessed with appropriate in vitro and in vivo studies, the indications here reported let to hypothesize an interesting potential for the successful use of these structures in novel orthopaedic implants, also considering the previous results obtained for the TT native structure [8], [18], [25]-[33].

REFERENCES

[1] K. Anselme, "Osteoblast adhesion on biomaterials," *Biomaterials*, vol. 21 (7), pp. 667-681, 2000.

[2] P. Heinl, L. Muller, C. Korner, R.F. Singer, F.A. Muller, "Cellular Ti6Al4V structures with interconnected macro porosity for bone implants fabricated by selective electron beam melting," *Acta Biomaterialia*, vol. 4 (5) pp. 1536-1544, 2008.

[3] M. Baleani, M. Viceconti, A. Toni, "The effect of sandblasting treatment on endurance properties of Titanium alloy hip prostheses," *Artificial Organs*, vol. 24 (4), pp. 296-299, 2000.

[4] A. Christensen, A. Lippincott, R. Kircher, "Qualification of electron beam melted (EBM) Ti6Al4V-ELI for orthopaedic implant applications", Golden, CO: Medical Modelling LLC, 2007.

[5] V.M. Goldberg, "Biology of grit blasted titanium alloy implants," *Clin Orthop Relat Res*, vol. 319, pp. 122-12, 1995.

[6] K.H. Frosch, F. Barvencik, V. Viereck, C.H. Lohmann, K. Dresing, J. Breme, E. Brunner, K.M. Sturmen, "Growth behavior, matrix production, and gene expression of human osteoblasts in defined cylindrical Titanium channels," *Journal of Biomedical Materials Research*, vol. 68A (2), pp. 325-334, 2004.

[7] V. Karageorgiou, D. Kaplan, "Porosity of 3D biomaterial scaffolds and osteogenesys," *Biomaterials*, vol. 26, pp. 5474-5491, 2005

[8] H.R. Bloch, S. Burelli, D. Devine, D. Arens, "Enhanced bone in-growth of the highly porous Trabecular Titanium^{TM}", in *Proceedings of 13th European Federation of National Association of Orthopaedics and Traumatology (EFORT)*, Berlin, 2012.

[9] M. Mour, D. Das, T. Winkler, E. Hoenig, G: Mielke, M.M. Morlock, A.F. Schilling, "Advances in porous biomaterials for dental and orthopaedic," *Applications Materials*, vol. 3, pp. 2947-2974, 2010.

[10] O. Cansizoglu, D. Harrysson, D. Cormier, H. West, T. Mahale, "Properties of Ti6Al4V non stochastic lattice structures fabricated via electron beam melting," *Material Science and Engineering*, vol. 492 (1-2), pp. 468-474, 2008.

[11] J.C.S. Pires, A.F.B. Braga, P.R. Mei, "Profile of impurities in polycrystalline silicon samples purified in an electron beam melting surface," *Solar Energy Materials & Solar Cells*, vol. 79 (3), pp. 347-355, 2003.

[12] A. Hershcovitch, "Non-vacuum electron beam welding through a plasma window," *Nuclear Instruments and Methods in Physics Research section B: Beam Interactions with Materials and Atoms*, vol. 241 (1-4), pp. 854-857, 2005.

[13] Q.F. Guan, H. Zou, A.M. Wu, S.Z. Hao, J.X. Zou, Y. Qin, C. Dong, Q.Y. Zhang, "Surface nanostructure and amorphous state of a low carbon steel induced by high current pulsed electron beam," *Surface and Coating Technology*, vol. 196 (1-3), pp. 145-149, 2005.

[14] S. Kalpakjian, S.R. Schmid, *Manufacturing Engineering and Technology*, Prentice Hall, Ed, 2009.

[15] P. Dalla Pria, M. Pressacco, E. Veronesi, "Nuove frontiere dell'osteointegrazione: Il trabecular titanium," *Sphera Medical Journal*, vol. 7, pp. 46-50, 2008.

[16] E. Marin, S. Fusi, M. Pressacco, L. Paussa, L. Fedrizzi, "Characterization of cellular solids in Ti6Al4V for orthopaedic implant applications: trabecular titanium," *Journal of mechanical behavior of biomedical materials*, vol. 3 (5), pp. 373-381, 2010.

[17] E. Marin, M. Pressacco, S. Fusi, A. Lanzutti, S. Turchet, L. Fedrizzi, "Characterization of commercially pure Ti Trabecular Titanium^{TM} structures," *Materials Science and Engineering C: Materials for biological applications*, vol. 33, pp. 2648-2656, 2013.

[18] D. Devine, D. Arens, S. Burelli, H.R. Bloch, L. Boure, "*In vivo* evaluation of the osteointegration of new highly porous Trabecular Titanium™", *Journal of Bone and Joint Surgery*, vol. 94-B(Suppl XXXVII), pp. 201.

[19] C.R. Ethier, C.A. Simmons, *Introductory biomechanics: from cells to organisms*, pp. 385-387, 2007.

[20] M. Ding, M. Dalastra, C.C. Danielsen, J. Kabel, I. Hvid, F. Linde, "Age variations in the properties of human tibial trabecular bone, *Journal of bone and joint surgery*, vol. 79, pp. 995-1002, 1197.

[21] ASTM F1147, "Standard Test Method for Tension Testing of Calcium Phosphate and Metallic Coatings", *ASTM international*, 2005.

[22] M.F. Ashby, R.F.M. Medalist, "The mechanical properties of cellular solids," *Metallurgical and Materials Transactions A*, vol. 14, pp. 1755-1769, 1983.

[23] M. F. Ashby, A. Evans, N. A. Fleck, L. J. Gibson, J. W. Hutchinson, H. N. G. Wadley, *Metal foams – a design guide*, Buttenworth Heineman, Ed: Elsevier, 2000.

[24] J.J. Callaghan, A.G. Rosenberg, H.E. Rubash, in *The adult hip*, 2nd ed. vol. 1, Lippincott Williams & Wilkins, 2007.

[25] V. Sollazzo, et al., "Genetic effects of Trabecular Titanium on MG-63 cell line: a genetic profiling evaluation," *ISRN materials science*, vol. 2011, ID 392763, 2011.

[26] G. Gastaldi, A. Asti, M.F. Scaffino, L. Visai, E. Saino, A.M. Cometa, F. Benazzo, "Human adipose-derived stem cells (hASCs) proliferate and differentiate in osteoblast-like cells on Trabecular Titanium scaffolds," *Journal of biomedical materials research part A*, vol. 94 (3), pp. 790-799, 2010.

[27] F. Benazzo, G. Gastaldi, J. Fontanta, L. Marullo, "Osteoinductive properties of Trabecular Titanium scaffolds on hASCs (adipose derived stem cells) ontogenetically differentiated," *Journal of bone and joint surgery*, vol. 94 (B), pp. 197 (suppl. XXXVII), 2012.

[28] M.F. Saffino, L. Botta, M.A. Avanzini, M. Mantelli, F. Benazzo, G. Gastaldi, "Use of adipose derived stem cells for orthopaedic tissue engineering: osteogenic differentiation on a Trabecular Titanium^{TM} 3-dimensional scaffold", in *Proceedings of the 1st International conference on adipose tissue (ICAT)*, Venice, 2011, pp. 97-98.

[29] V. Sollazzo, A. Plamieri, L. Massari, F. Clarinci, "Genetic effects of Trabecular Titanium on cells MG-63 line: an in vitro study," *Journal of orthopaedic traumatology*, vol. 13 (1), pp. 107, 2012.

[30] E. Marin, L. Fedrizzi, M. Regis, M. Pressacco, L. Zagra, S. Fusi, "Stability enhancement of prosthetic implants: friction analysis of Trabecular Titanium"; *Hip international*, vol. 22 (4), pp. 427-428, 2012.

[31] F. Benazzo, L. Botta, M.F. Scaffino, L. Caliogna, M. Marullo, S. Fusi, G. Gastaldi, "Trabecular Titanium can induce in vitro osteogenic differentiation of human adipose derived stem cells without osteogenic factors," *Journal of biomedical materials research part A*, [Epub ahead of print], 2013.

[32] L. Massari, A. Causero, P. Rossi, P.P. Grillo, A. Bistolfi, G. Gigliofiorito, C. Pari, A. Francescotto, P. Tosco, D. Deledda, G. Carli, S. Burelli, "Multicentre prospective densitometric study on Trabecular Titanium^{TM} osseointegration," *Bone joint journal*, vol. 95-B (suppl. 34), pp. 416, 2013.

[33] L. Perticarini, L. Piovani, S.M.P. Rossi, A. Combi, A. Padolino, F. Benazzo, "242 cups in Trabecular Titanium: short-term follow-up," *Journal of orthopaedic traumatology*, vol. 12 (suppl. 1), pp. 147, 2011.